Förster, H.-J., Bindi, L., Grundmann, G., Stanley, C. (2018): Cerromojonite, CuPbBiSe3, from El Dragón (Bolivia): A New Member of the Bournonite Group. - *Minerals*, *8*, 10.

DOI: http://doi.org/10.3390/min8100420

minerals

MDPI

Article

Cerromojonite, $CuPbBiSe_3$, from El Dragón (Bolivia): A New Member of the Bournonite Group

Hans-Jürgen Förster [1,*], Luca Bindi [2], Günter Grundmann [3] and Chris J. Stanley [4]

1 Helmholtz Centre Potsdam German Research Centre for Geosciences GFZ, DE-14473 Potsdam, Germany
2 Dipartimento di Scienze della Terra, Università degli Studi di Firenze, Via G. La Pira 4, I-50121 Firenze, Italy; luca.bindi@unifi.it
3 Chair of Engineering Geology, Technical University Munich, Arcisstr. 23, DE-80333 Munich, Germany; grundmann.g@gmx.de
4 Department of Earth Sciences, Natural History Museum, Cromwell Road, London SW7 5BD, UK; c.stanley@nhm.ac.uk
* Correspondence: forhj@gfz-potsdam.de; Tel.: +49-0331-288-28843

Received: 25 July 2018; Accepted: 30 August 2018; Published: 21 September 2018

Abstract: Cerromojonite, ideally $CuPbBiSe_3$, represents a new selenide from the El Dragón mine, Department of Potosí, Bolivia. It either occurs as minute grains (up to 30 μm in size) in interstices of hansblockite/quijarroite intergrowths, forming an angular network-like intersertal texture, or as elongated, thin-tabular crystals (up to 200 μm long and 40 μm wide) within lath-shaped or acicular mineral aggregates (interpreted as pseudomorphs) up to 2 mm in length and 200 μm in width. It is non-fluorescent, black, and opaque, with a metallic luster and black streak. It is brittle, with an irregular fracture, and no obvious cleavage and parting. In plane-polarized incident light, cerromojonite is grey to cream-white, and weakly pleochroic, showing no internal reflections. Between crossed polarizers, cerromojonite is weakly anisotropic, with rotation tints in shades of brown and grey. Lamellar twinning on {110} is common. The reflectance values in air for the COM standard wavelengths (R_1 and R_2) are: 48.8 and 50.3 (470 nm), 48.2 and 51.8 (546 nm), 47.8 and 52.0 (589 nm), and 47.2 and 52.0 (650 nm). Electron-microprobe analyses yielded a mean composition of: Cu 7.91, Ag 2.35, Hg 7.42, Pb 16.39, Fe 0.04, Ni 0.02, Bi 32.61, Se 33.37, total 100.14 wt %. The empirical formula (based on 6 atoms *pfu*) is $(Cu_{0.89}Hg_{0.11})_{\Sigma=1.00}(Pb_{0.56}Ag_{0.16}Hg_{0.15}Bi_{0.11}Fe_{0.01})_{\Sigma=0.99}Bi_{1.00}Se_{3.01}$. The ideal formula is $CuPbBiSe_3$. Cerromojonite is orthorhombic (space group $Pn2_1m$), with a = 8.202(1) Å, b = 8.741(1) Å, c = 8.029(1) Å, V = 575.7(1) Å^3, Z = 4. Calculated density is 7.035 g·cm^{-3}. The five strongest measured X-ray powder diffraction lines (d in Å (I/I_0) (*hkl*)) are: 3.86 (25) (120), 2.783 (100) (122), 2.727 (55) (212), 2.608 (40) (310), and 1.999 (25) (004). Cerromojonite is a new member of the bournonite group, representing the Se-analogue of součekite, $CuPbBi(S,Se)_3$. It is deposited from strongly oxidizing low-T hydrothermal fluids at a f_{Se2}/f_{S2} ratio >1, both as primary and secondary phase. The new species has been approved by the IMA-CNMNC (2018-040) and is named for Cerro Mojon, the highest mountain peak closest to the El Dragón mine.

Keywords: cerromojonite; selenium; copper; lead; mercury; bismuth; součekite; bournonite group; El Dragón; Bolivia

1. Introduction

The Bolivian Andes host two mineralogically important selenide occurrences: Pacajake, district of Hiaco de Charcas; and El Dragón, Province of Antonio Quijarro; both in the Department of Potosí. The El Dragón mineralization represents a multi-phase assemblage of primary and secondary minerals, among which Se-bearing phases are the most prominent. It is the type

locality for eldragónite, $Cu_6BiSe_4(Se_2)$ [1]; favreauite, $PbBiCu_6O_4(SeO_3)_4(OH)\cdot H_2O$ [2]; grundmannite, $CuBiSe_2$ [3]; hansblockite, $(Cu,Hg)(Bi,Pb)Se_2$ [4]; alfredopetrovite, $Al_2(Se^{4+}O_3)_3\cdot 6H_2O$ [5]; quijarroite, $Cu_6HgPb_2Bi_4Se_{12}$ [6]; and also contains the lately discovered rare orthorhombic dimorph of $CuSe_2$, petříčekite [7]. A comprehensive survey of the geology and origin of the El Dragón Se-mineralization was published by Grundmann and Förster (2017) [8], who also provided a full list of minerals recorded as from this locality.

This paper provides a description of a new species in the Cu–Hg–Pb–Bi–Se system, cerromojonite, ideally $CuPbBiSe_3$, from El Dragón. This new species and its name have been approved by the Commission on New Minerals, Nomenclature and Classification (CNMNC) of the IMA, proposal 2018-040. The X-rayed crystal is preserved by one of the authors (L.B.) at the Dipartimento di Scienze della Terra, Università degli Studi di Firenze. The polished section, from which the crystal was extracted (holotype), is housed in the collections of the Natural History Museum, London, with the catalogue number BM 2018, 11. Cotype material, consisting of another cerromojonite-bearing polished section, is deposited within the Mineralogical State Collection Munich (Mineralogische Staatssammlung München, Museum "Reich der Kristalle"), with the inventory number MSM 73583.

The species is named for Cerro Mojon, the highest mountain peak nearest to El Dragón (4292 m above sea level), located about 800 m northeast of the mine.

Unnamed phase "C", described at El Dragón already in 2016 [3], for which no structural data were obtained, compositionally resembles cerromojonite. A species similar to cerromojonite was speculated to occur in carbonate veins in the Schlema–Alberoda U–Se–polymetallic deposit (Erzgebirge, Germany), forming tiny inclusions which are intimately intergrown with berzelianite [9,10]. However, neither compositional data of pure material nor structural data were provided for this material.

2. Geology

The abandoned El Dragón mine is situated in the Cordillera Oriental (southwestern Bolivia), about 30 km southwest of Cerro Rico de Potosí. It is located at 19°49′23.90″ S (latitude), 65°55′00.60″ W (longitude), at an altitude of 4160 m above sea level. The adit of the mine is on the orographic left side of the Rio Jaya Mayu, cutting through a series of thinly-stratified, pyrite-rich black shales, and reddish-grey, hematite-bearing siltstones, dipping 40° to the north. The almost vertical ore vein is located in the center of a 1.5-m-wide shear zone (average trend 135 degrees). In 1988, the selenium mineralization consisted of a single vein of small longitudinal extension (maximum 15-m-long gallery), ranging mostly from 0.5 to 2 cm in thickness.

3. Physical and Optical Properties

Cerromojonite occurs within two different mineral assemblages, which are interpreted as representing genetically distinct types.

Type-I cerromojonite (maximum grain size ~30 μm) crystallized in the interstices of quijarroite/hansblockite intersertal intergrowths, partly together with penroseite ($NiSe_2$), klockmannite (CuSe), watkinsonite ($Cu_2PbBi_4Se_8$), clausthalite (PbSe), and, more rarely, petrovicite ($Cu_3HgPbBiSe_5$) (Figure 1). These aggregates are cemented by umangite (Cu_3Se_2) and klockmannite. They were deposited at the surfaces of krut'aite–penroseite ($CuSe_2$–$NiSe_2$) solid solutions.

Cerromojonite type-II occurs within lath-shaped or acicular mineral aggregates (up to 2 mm in length and 200 μm in width), that are interpreted as pseudomorphs after the above described intersertal aggregates (Figure 2). In this case, it forms elongated thin-tabular crystals (up to 200 μm long and 40 μm wide), intimately (subparallel) intergrown with watkinsonite, and less frequently, quijarroite (Figure 3), clausthalite, unnamed $CuNi_2Se_4$ [11], and (according to energy-dispersive electron-microprobe analysis) two new Cu–(Ag)–Hg–Pb–Bi selenides (Figure 4), which were all cemented by klockmannite. These pseudomorphs occasionally show parallel intergrowth of grains, which is implied by the serrated prismatic grain surfaces. They are usually deposited in interstices in brecciated krut'aite–penroseite ($CuSe_2$–$NiSe_2$) grains. The appearance of the cerromojonite grains

resembles a spinifex texture, indicating fast crystallization. Type-II cerromojonite and associated minerals are themselves altered by late klockmannite, fracture-filling chalcopyrite, covellite, goethite, endmember petříčekite and krut'aite ($CuSe_2$), and native selenium (Figure 5).

Cerromojonite is black in color and possesses a black streak. The mineral is opaque in transmitted light, exhibits a metallic luster, and is non-fluorescent. No cleavage and parting is observed, and the fracture is irregular. Density and Mohs hardness could not be measured owing to the small crystal size. The calculated density is 7.035 g/cm^3 (for $Z = 4$), based on the empirical formula (see below) and the unit-cell parameters derived from X-ray single-crystal refinement.

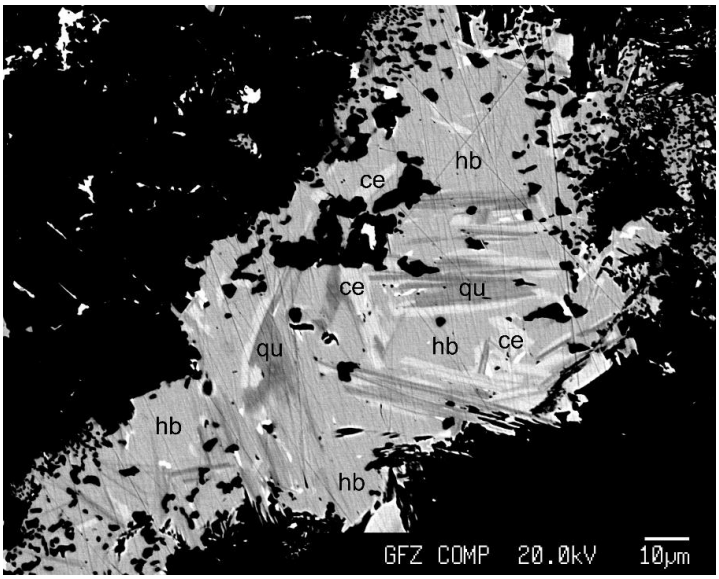

Figure 1. Back-scattered electron (BSE) image of type-I cerromojonite intergrown with hansblockite and quijarroite, forming an angular network-like intersertal texture. Abbreviations: ce = cerromojonite, hb = hansblockite, qu = quijarroite.

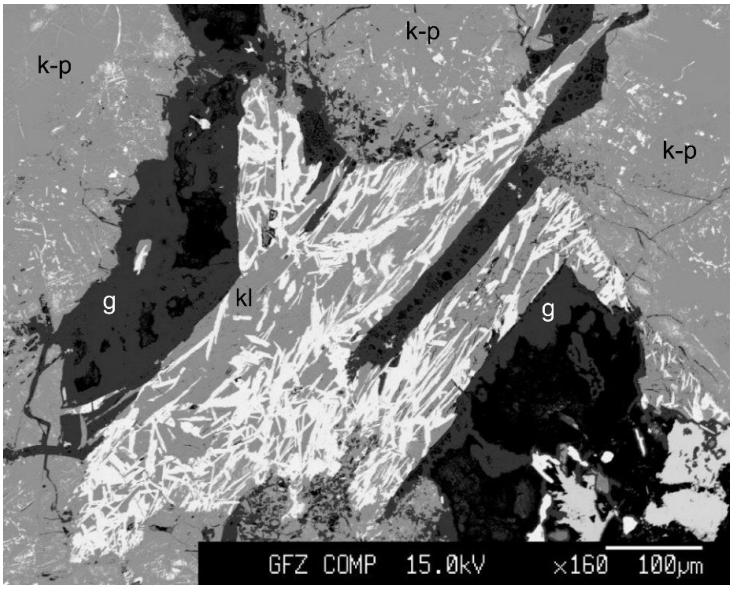

Figure 2. BSE image showing a pseudomorph composed of bright type-II cerromojonite, watkinsonite, and quijarroite, cemented by medium-grey klockmannite. Abbreviations: k–p = krut'aite–penroseite solid solutions, kl = klockmannite, g = goethite.

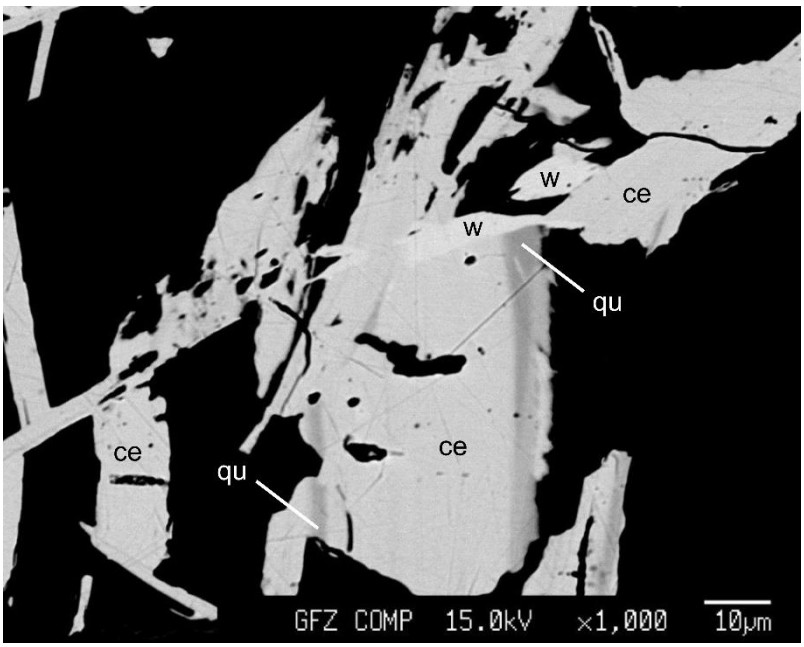

Figure 3. BSE image of type-II cerromojonite (ce) intergrown with quijarroite (qu) and watkinsonite (w).

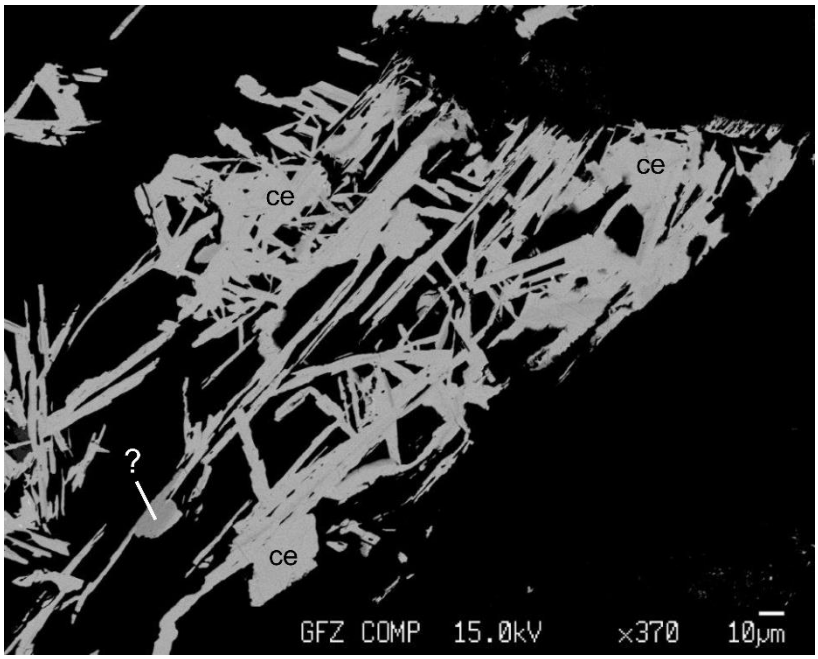

Figure 4. BSE image of parallel-intergrown type-II cerromojonite (ce) grains with darker domains of an unknown Cu–(Ag)–Hg–Pb–Bi selenide. The biggest grain of this potentially new species is marked by a question mark.

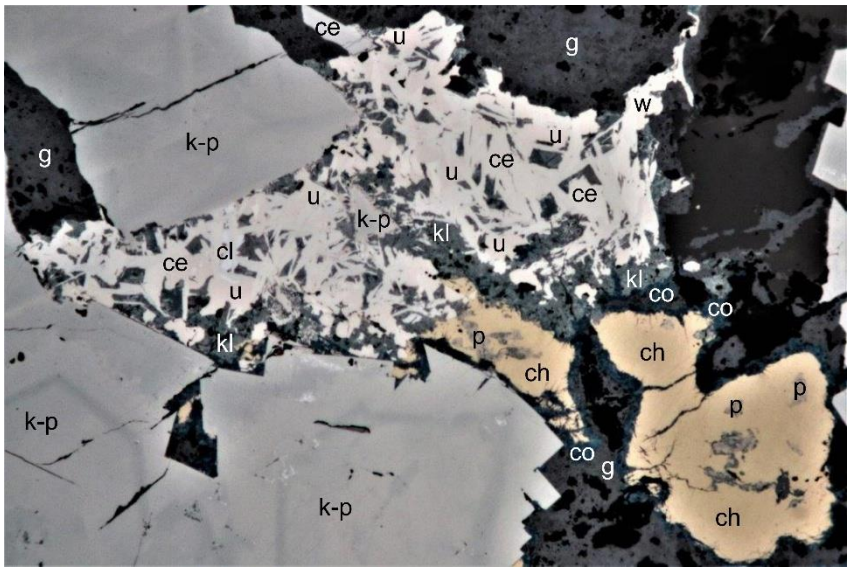

Figure 5. Type-II cerromojonite-bearing pseudomorph progressively altered by goethite and sulfides (reflected light, horizontal field of view is 500 μm). Abbreviations: ce = cerromojonite, ch = chalcopyrite, cl = clausthalite, co = covellite, g = goethite, kl = klockmannite, k–p = krut'aite–penroseite solid solution, p = penroseite, w = watkinsonite, u = unnamed $CuNi_2Se_4$.

In plane-polarized incident light, cerromojonite is grey to cream-white. In the assemblage with klockmannite and watkinsonite, it is weakly pleochroic or bireflectant. The mineral does not show any internal reflections. Between crossed polarizers, cerromojonite is weakly anisotropic, with rotation tints in shades of brown and grey (Figure 6). Twinning of cerromojonite is expressed either by distinct sharp polysynthetic lamellae (Figure 7) or by finely divided twinning in fan-shaped aggregates.

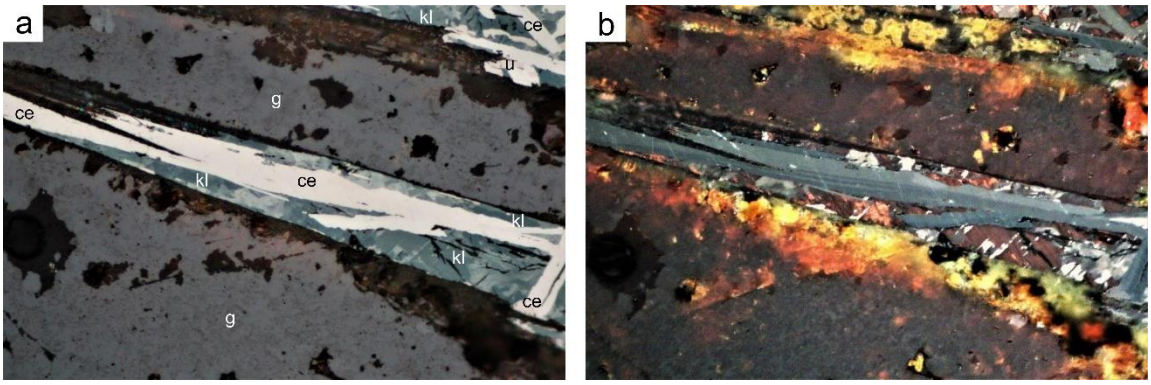

Figure 6. Type-II cerromojonite and associated minerals in plane polarized light (**a**), and at partially crossed polarizers (**b**) (horizontal field of view is 200 μm). Lamellar twinning on {110} of cerromojonite is well displayed in (**b**). Abbreviations: ce = cerromojonite, g = goethite, kl = klockmannite, u = unnamed $CuNi_2Se_4$.

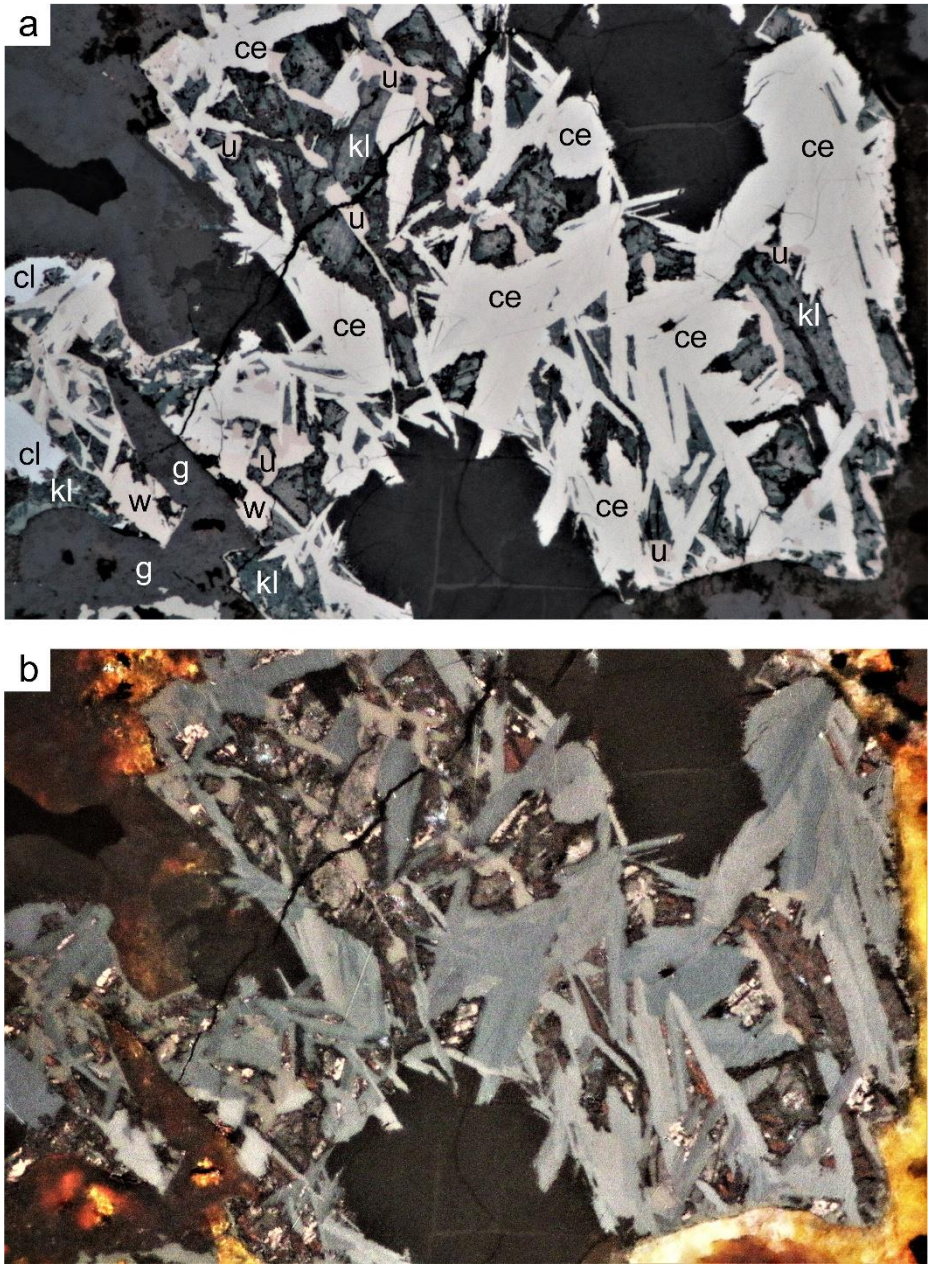

Figure 7. Type-II cerromojonite associated with klockmannite, unnamed $CuNi_2Se_4$, clausthalite, and later-formed goethite in reflected light: (**a**) 1 polarizer, (**b**) partially crossed polarizers. Horizontal field of view is 200 μm. Abbreviations: ce = cerromojonite, kl = klockmannite, w = watkinsonite, cl = clausthalite, u = unnamed $CuNi_2Se_4$, g = goethite.

Quantitative reflectance measurements were performed in air relative to a WTiC standard (Zeiss number 314) by means of a J & M TIDAS diode array spectrometer (J & M Analytik AG, Essingen, Germany), running ONYX software (Version 1.1, Cavendish Instruments Ltd., Sheffield, UK) on a Zeiss Axioplan ore microscope (Carl Zeiss AG, Oberkochen, Germany) (Table 1, Figure 8). Measurements were made on unoriented grains at extinction positions leading to the designation of R_1 (minimum) and R_2 (maximum).

Table 1. Reflectance data.

λ (nm)	R_1 (%)	R_2 (%)	λ (nm)	R_1 (%)	R_2 (%)
400	47.0	48.0	560	48.1	51.9
420	47.2	48.6	580	47.9	52.0
440	47.5	49.3	600	47.7	52.1
460	47.8	50.0	620	47.5	52.1
480	48.1	50.6	640	47.3	52.0
500	48.3	51.1	660	47.1	51.9
520	48.3	51.5	680	46.9	51.7
540	48.3	51.7	700	46.8	51.6

Reflectance percentages (R_1 and R_2) for the four Commission on Minerals (COM) wavelengths are: 48.8, 50.3 (470 nm); 48.2, 51.8 (546 nm); 47.8, 52.0 (589 nm); 47.2, 52.0 (650 nm).

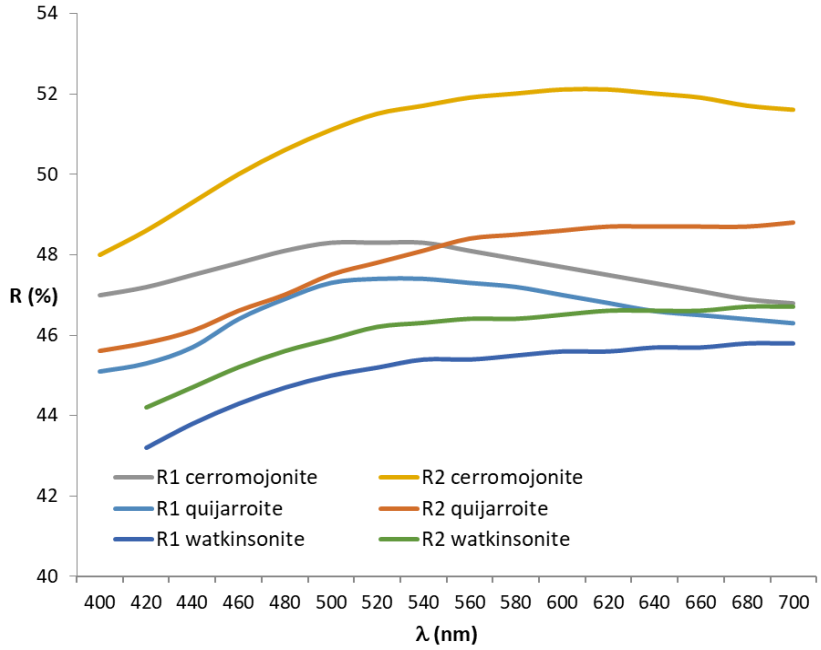

Figure 8. Reflectance spectra of type-II cerromojonite and its most frequently associated Cu–Bi selenides: quijarroite [6] and watkinsonite [12].

4. Chemical Data

Cerromojonite was checked for concentrations of Cu, Ag, Pb, Hg, Fe, Co, Ni, As, Sb, Bi, S, and Se. Twenty-four spot analyses of type-II cerromojonite from the holotype section, were performed using a JEOL JXA-8230 electron microprobe (WDS mode, 20 kV, 20 nA, 1–2 μm beam size) (JEOL Ltd., Akishima, Japan). The composition of the grain used for the structural study corresponds chemically to the other grains analyzed by microprobe, which were proved to be homogeneous within 2σ standard deviations of the analyzed elements. The counting time on the peak was 20 s, with half that time on background on both sites of the peak. The following standards, emission lines, and analyzing crystals (in parentheses) were used: Cu–eskebornite, *Kα* (LIFL); Ag–bohdanowiczite, *Lα* (PETJ); Pb–galena, *Mα* (PETH); Hg–cinnabar, *Lα* (LIFL); Fe–chalcopyrite, *Kα* (LIFL); Co–cobaltite, *Kα* (LIFL); Ni–pentlandite, *Kα* (LIFL); As–skutterudite, *Lα* (TAP); Sb–skutterudite, *Lα* (PETJ); Bi–synthetic Bi_2Se_3, *Mα* (PETH); S–chalcopyrite, *Kα* (PETJ); Se–synthetic Bi_2Se_3, *Kα* (LIFL). The software-implemented PRZ (XPP metal) data-correction routine (JEOL EPMA version 10) (JEOL Ltd., Akishima, Japan), which is based on the $\phi(\rho Z)$ method [13], was used for data processing. Table 2 compiles the analytical data for cerromojonite (means of 24 spot analyses, ranges, and standard deviations). Table 3 provides a selection of results from microprobe spot analyses of cerromojonite, together with the elemental detection limits (d.l.).

Table 2. Chemical data for cerromojonite.

Element	Mean	Range	e.s.d.
Cu (wt %)	7.91	7.40–8.16	0.18
Ag	2.35	2.16–2.54	0.11
Hg	7.42	7.19–7.60	0.10
Pb	16.39	16.15–16.77	0.13
Fe	0.04	0.00–0.18	0.04
Ni	0.02	0.00–0.18	0.04
Bi	32.61	32.19–32.91	0.20
Se	33.37	32.93–33.81	0.24
Total	100.11	99.24–100.79	0.42

$(Cu_{0.89}Hg_{0.11})_{\Sigma = 1.00}(Pb_{0.56}Ag_{0.16}Hg_{0.15}\ Bi_{0.11}\ Fe_{0.01})_{\Sigma = 0.99}Bi_{1.00}Se_{3.01}$ is the empirical formula of cerromojonite (based on 6 atoms *pfu*). The ideal formula of the mineral is CuPbBiSe3, corresponding to the ideal contents of the elements (in wt %) Cu 8.87, Pb 28.92, Bi 29.15, Se 33.06, sum 100.00.

Table 3. Representative results of electron-microprobe spot analyses of cerromojonite.

Element	d.l. (ppm)	1	2	3	4	5	6
Cu (wt %)	250	7.40	7.75	8.09	8.03	7.91	7.91
Ag	200	2.45	2.54	2.30	2.33	2.54	2.27
Hg	1100	7.48	7.46	7.37	7.38	7.32	7.33
Pb	400	16.29	16.31	16.50	16.46	16.34	16.36
Fe	150	b.d.l.	0.14	b.d.l.	b.d.l.	b.d.l.	b.d.l.
Ni	200	b.d.l.	0.04	b.d.l.	b.d.l.	0.11	0.03
Bi	300	32.74	32.76	32.78	32.80	32.42	32.51
Se	800	33.48	33.27	33.58	33.31	33.07	33.56
Total		99.86	100.28	100.64	100.22	99.74	99.98
Cu (*a.p.f.u.*)		0.84	0.87	0.90	0.90	0.89	0.89
Ag		0.16	0.17	0.15	0.15	0.17	0.15
Hg		0.27	0.26	0.26	0.26	0.26	0.26
Pb		0.56	0.56	0.56	0.57	0.56	0.56
Fe		-	0.02	-	-	-	-
Ni		-	-	-	-	0.01	-
Bi		1.12	1.12	1.11	1.12	1.11	1.11
Se		3.04	3.00	3.01	3.01	2.99	3.03

a.p.f.u. = atoms per formula unit; b.d.l. = below limit of detection.

5. X-ray Crystallography and Description of the Crystal Structure

X-ray powder diffraction data (Table 4) were obtained from the same fragment used for the single-crystal study (see below), with an Oxford Diffraction Excalibur PX Ultra diffractometer (Oxford Diffraction, Oxford, UK), fitted with a 165 mm diagonal Onyx CCD detector, and using copper radiation (Cu$K\alpha$, λ = 1.54138 Å). The working conditions were 40 kV and 40 mA, with 1 hour of exposure; the detector-to-sample distance was 7 cm.

Table 4. Measured and calculated X-ray powder diffraction data (d in Å) for cerromojonite. The strongest measured diffraction lines are given in bold.

hkl	d_{meas}	I_{meas}	d_{calc}	I_{calc}
020	-	-	4.3705	4
-	4.08	10	4.1010	9
002	4.00	20	4.0145	15
120	**3.86**	**25**	**3.8571**	**20**
210	3.70	10	3.7127	9
112	3.32	10	3.3333	9
220	2.991	10	2.9906	10
022	-	-	2.9565	6
202	-	-	2.8688	7
122	**2.783**	**100**	**2.7814**	**100**
130	2.747	10	2.7456	12
212	**2.727**	**55**	**2.7257**	**50**
310	**2.608**	**40**	**2.6093**	**37**
222	-	-	2.3983	5
320	-	-	2.3178	3
132	-	-	2.2663	9
312	-	-	2.1878	5
040	2.186	10	2.1853	14
004	**1.999**	**25**	**2.0073**	**21**
330	1.992	20	1.9937	21
042	-	-	1.9193	4
142	1.867	10	1.8688	12
412	1.788	20	1.7875	22
332	-	-	1.7856	6
124	-	-	1.7806	4
242	-	-	1.7384	6
422	-	-	1.6849	3
224	-	-	1.6666	3
134	-	-	1.6204	4
314	1.592	20	1.5910	14
252	1.494	10	1.4928	10
044	-	-	1.4783	7
522	-	-	1.4344	4
530	-	-	1.4294	4
334	1.415	10	1.4145	12
260	-	-	1.3728	4
600	-	-	1.3670	4
126	-	-	1.2642	6
452	-	-	1.2628	8
216	-	-	1.2589	3
534	-	-	1.1644	3
264	-	-	1.1331	4
604	-	-	1.1299	4
416	-	-	1.1115	3
722	-	-	1.0893	5
182	-	-	1.0457	3
456	-	-	0.9434	3

Note: calculated diffraction pattern obtained with the atom coordinates reported in Table 6 (only reflections with $I_{rel} \geq 3$ are listed).

The program *Crysalis* RED [14] was used to convert the observed diffraction rings to a conventional powder diffraction pattern. Least squares refinement gave the following orthorhombic unit-cell values: a = 8.2004(6) Å, b = 8.7461(5) Å, c = 8.0159(5) Å, V = 574.91(5) Å^3, and Z = 4.

A small crystal (0.040 × 0.055 × 0.060 mm^3) of type-II cerromojonite was handpicked from the holotype specimen (it is registered under the number #123 in the mineralogical collection of one of the Authors, G.G.). The crystal was preliminarily examined with a Bruker-Enraf MACH3 single-crystal

diffractometer (Bruker, Karlsruhe, Germany), using graphite-monochromatized Mo$K\alpha$ radiation. Single-crystal X-ray diffraction intensity data were collected using an Oxford Diffraction Xcalibur diffractometer equipped with an Oxford Diffraction CCD detector, with graphite-monochromatized Mo$K\alpha$ radiation (λ = 0.71073 Å). The data were integrated, and corrected for standard Lorentz and polarization factors, with the *CrysAlis* RED package [12]. The program ABSPACK in *CrysAlis* RED [12] was used for the absorption correction. Table 5 reports details of the selected crystal, data collection, and refinement.

Table 5. Data and experimental details for the selected cerromojonite crystal.

Crystal Data	
Ideal formula	$CuPbBiSe_3$
Crystal size (mm^3)	0.040 × 0.055 × 0.060
Form	Block
Color	Black
Crystal system	Orthorhombic
Space group	$Pn2_1m$
a (Å)	8.202(1)
b (Å)	8.741(1)
c (Å)	8.029(1)
V ($Å^3$)	575.7(1)
Z	4
Data Collection	
Instrument	Oxford Diffraction Xcalibur 3
Radiation type	Mo$K\alpha$ (λ = 0.71073 Å)
Temperature (K)	293(3)
Detector to sample distance (cm)	6
Number of frames	889
Measuring time (s)	50
Maximum covered 2θ (°)	59.30
Absorption correction	multi-scan [12]
Collected reflections	3504
Unique reflections	1359
Reflections with $F_o > 4\sigma(F_o)$	701
R_{int}	0.0356
R_σ	0.0412
Range of h, k, l	$0 \leq h \leq 11$, $-12 \leq k \leq 8$, $0 \leq l \leq 10$
Refinement	Full-matrix least squares on F^2
Final R_1 [$F_o > 4\sigma(F_o)$]	0.0256
Final R_1 (all data)	0.0315
S	1.09
Number refined parameters	68
$\Delta\rho_{max}$ (e $Å^{-3}$)	1.81
$\Delta\rho_{min}$ (e $Å^{-3}$)	−2.06

Statistical tests ($|E^2 - 1| = 0.821$) and systematic absences agreed with the acentric space group $Pn2_1m$. The crystal structure was refined starting from the atomic coordinates of bournonite [15]. Given the observed larger unit-cell volume of cerromojonite (i.e., 575.7 $Å^3$) compared to bournonite (i.e., 552.3 $Å^3$; [15]), the site occupancy factor (s.o.f.) at the crystallographic sites was allowed to vary (Pb vs. Ag and Bi vs. Ag for the Pb and Bi sites; Cu vs. Hg for the Cu site; Se vs. S for the anionic site), using scattering curves for neutral atoms taken from the International Tables for Crystallography [16]. After several cycles of anisotropic refinement, a final R_1 = 0.0256 for 701 reflections with $F_o > 4\ \sigma(F_o)$ and 68 refined parameters was achieved (0.0315 for all 1359 reflections). Atomic coordinates, site occupancies, and equivalent isotropic displacement parameters are listed in Table 6, whereas anisotropic displacement parameters are given in Table 7. Selected bond distances and

bond-valence sums are provided in Table 8. The Crystallographic Information File (CIF) is available as Supplementary Material.

Table 6. Atoms, site occupancy factors (s.o.f.), fractional atomic coordinates (x, y, z), and equivalent isotropic displacement parameters (U_{eq}, Å^2) for the selected cerromojonite crystal.

Atom	s.o.f.	x	y	z	U_{eq}
Pb1	$Pb_{0.80(2)}Ag_{0.20}$	0.07291(13)	0.9709(3)	0	0.0108(5)
Pb2	$Pb_{0.74(2)}Ag_{0.26}$	0.56972(12)	0.1758(3)	$\frac{1}{2}$	0.0115(5)
Bi1	$Bi_{1.00}$	0.07446(12)	0.9807(2)	$\frac{1}{2}$	0.0118(4)
Bi2	$Bi_{1.00}$	0.55647(12)	0.1819(2)	0	0.0134(4)
Cu	$Cu_{0.870(8)}Hg_{0.130}$	0.27526(17)	0.42151(15)	0.2439(3)	0.0120(6)
Se1	$Se_{1.00}$	0.2450(3)	0.2494(4)	0	0.0103(6)
Se2	$Se_{1.00}$	0.2316(3)	0.2595(4)	$\frac{1}{2}$	0.0105(6)
Se3	$Se_{1.00}$	0.08564(19)	0.65945(19)	0.2374(4)	0.0102(4)
Se4	$Se_{1.00}$	0.57919(18)	0.4826(2)	0.2675(4)	0.0096(4)

Table 7. Anisotropic displacement parameters (U) of the atoms for the selected cerromojonite crystal.

Atom	U^{11}	U^{22}	U^{33}	U^{12}	U^{13}	U^{23}
Pb1	0.0116(7)	0.0118(11)	0.0089(7)	0.0005(5)	0.000	0.000
Pb2	0.0102(8)	0.0135(10)	0.0107(8)	−0.0008(7)	0.000	0.000
Bi1	0.0123(6)	0.0122(10)	0.0110(7)	−0.0001(4)	0.000	0.000
Bi2	0.0149(6)	0.0136(8)	0.0118(6)	−0.0001(6)	0.000	0.000
Cu	0.0131(8)	0.0125(7)	0.0104(9)	0.0007(4)	0.0007(7)	−0.0003(10)
Se1	0.0108(11)	0.0119(16)	0.0081(12)	−0.0007(10)	0.000	0.000
Se2	0.0114(10)	0.0111(15)	0.0089(12)	0.0001(10)	0.000	0.000
Se3	0.0101(7)	0.0108(7)	0.0096(11)	−0.0004(6)	0.0000(7)	0.0036(13)
Se4	0.0111(7)	0.0108(7)	0.0070(12)	−0.0002(7)	−0.0009(6)	−0.0004(12)

Table 8. Bond distances (in Å) and bond valence sums (BVS in valence units) in the structure of cerromojonite.

Pb1-Se1	2.814(4)	Bi2-Se1	2.622(3)
Pb1-Se3 (×2)	2.975(3)	Bi2-Se4 (×2)	2.785(3)
Pb1-Se2	3.107(3)	Bi2-Se4 (×2)	3.395(3)
Pb1-Se3 (×2)	3.334(3)	Bi2-Se3 (×2)	3.620(3)
Pb1-Se4 (×2)	3.408(3)	BVS	3.22
BVS	1.93		
		Cu-Se1	2.482(3)
Pb2-Se2	2.868(3)	Cu-Se2	2.522(3)
Pb2-Se4 (×2)	2.993(3)	Cu-Se4	2.557(2)
Pb2-Se4 (×2)	3.268(3)	Cu-Se3	2.598(2)
Pb2-Se3 (×2)	3.412(3)	BVS	1.29
BVS	1.62		
Bi1-Se2	2.757(4)		
Bi1-Se3 (×2)	2.793(3)		
Bi1-Se1	3.314(3)		
Bi1-Se3 (×2)	3.519(3)		
Bi1-Se4 (×2)	3.563(3)		
BVS	2.96		

v.u. = valence units.

The crystal structure of cerromojonite (Figure 9) is identical to those of the three members of the bournonite group: bournonite ($PbCuSbS_3$), seligmannite ($PbCuAsS_3$), and součekite ($PbCuBi(S,Se)_3$). It consists of $^{[7,9]}$Pb-polyhedra, $^{[3+2,3+3]}$Bi-polyhedra, and $CuSe_4$ tetrahedra, which share corners and edges to form a 3-dimensional framework; $CuSe_4$ tetrahedra share corners to form chains parallel

to [001] (Figure 10). The two Pb sites were found to exhibit a mean electron number of 75.0 and 72.9 electrons, respectively. According to their structural environments, and taking into account the bond-valence sums calculated using the parameters of Breese and O'Keeffe [17], the following site-populations were determined: $Pb_{0.52}Ag_{0.20}Bi_{0.16}Hg_{0.12}$ and $Pb_{0.60}Hg_{0.16}Ag_{0.12}Bi_{0.05}\square_{0.07}$. Bi-sites were thought to be filled by Bi only (according to the site-occupancy refinement), whereas the Cu site (35.6 electrons) was determined to be $Cu_{0.88}Hg_{0.12}$. Such a cation distribution is in agreement with the observed bond distances.

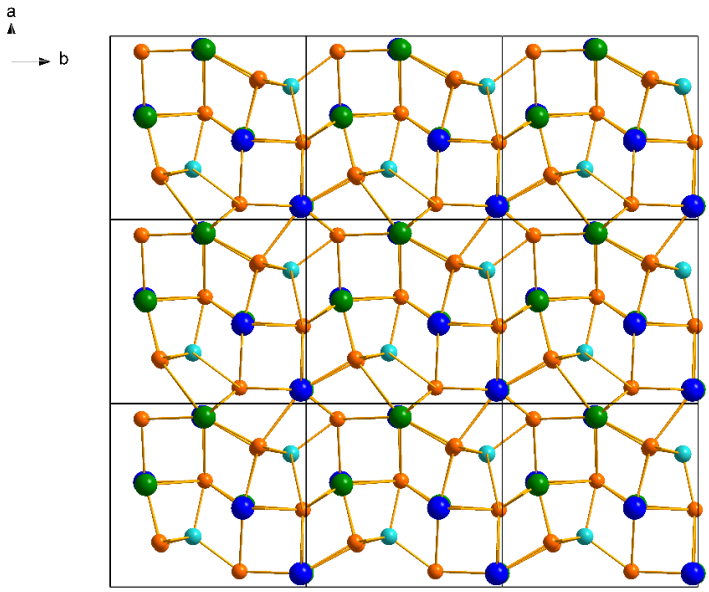

Figure 9. The crystal structure of cerromojonite projected down [001] (six unit-cells). The unit-cell and orientation of the figure are outlined. Symbols: Bi = green dots, Pb = blue dots, Cu = light blue dots, Se = orange dots.

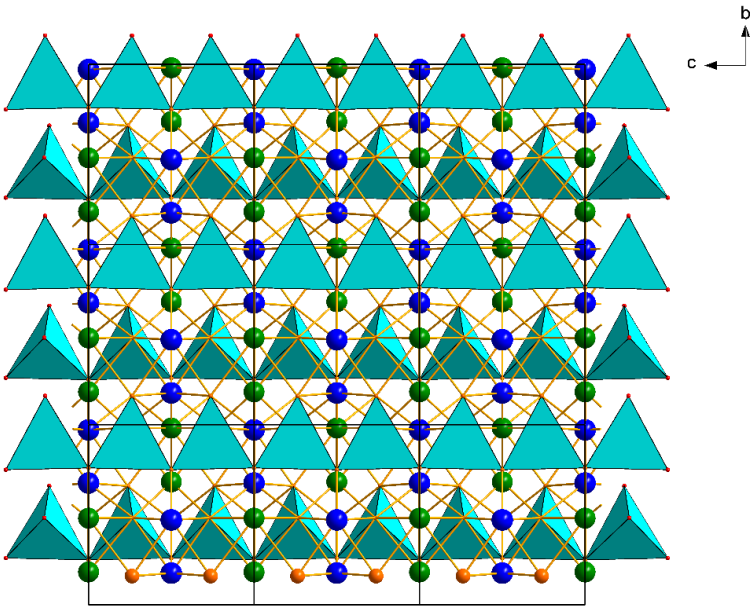

Figure 10. The crystal structure of cerromojonite projected down [100] (six unit-cells). Symbols as in Figure 9. $CuSe_4$ tetrahedra are depicted as light blue polyhedra. The unit-cell and orientation of the figure are outlined.

The overall crystallochemical formula, as obtained through the single-crystal X-ray diffraction study, is $[Cu_{0.880}Hg_{0.120}]Bi[Pb_{0.560}Ag_{0.155}Hg_{0.142}Bi_{0.107}\square_{0.036}]Se_3$ ($Z = 4$), and is in excellent agreement with that obtained from electron microprobe data.

6. Discussion

Cerromojonite is a new member of the bournonite group and represents the Se-analogue of součekite, $CuPbBi(S,Se)_3$ [12,18]. Interestingly, whereas previously analyzed součekite always contained appreciable amounts of Se (together with minor Te) substituting for S, cerromojonite from El Dragón is practically devoid of S, containing S at concentrations below its detection limit of ~200 ppm. Moreover, součekite is characterized by an almost ideal occupancy of the Cu-, Pb-, and Bi-sites, in contrast to cerromojonite, where significant amounts of other cations, in particular Ag and Hg, entered the structure.

Conclusions on the physico-chemical environment of cerromojonite formation could be drawn from the associated Cu selenides. It is apparent that type-I cerromojonite crystallized together with umangite and klockmannite, implying that selenium fugacities (f_{Se2}) fluctuated around values defined by the umangite–klockmannite univariant reaction. Type-II cerromojonite precipitated in equilibrium with klockmannite, outside the stability fields of umangite and krut'aite. At $T = 100$ °C, a temperature typical for the formation of vein-type selenide deposits, and an elevated oxygen fugacity defined by the magnetite–hematite buffer, these paragenetic relations are consistent with the range of $\log f_{Se2}$ between −14.6 and −11.6 [19]. The absence of krut'aite and sulfides (chalcopyrite, pyrite) define the maximum log of sulfur fugacity (f_{S2}) to be roughly −19.

Supplementary Materials: The following are available online at http://www.mdpi.com/2075-163X/8/10/420/s1, CIF: Cerromojonite.

Author Contributions: G.G. collected the samples and manufactured the polished sections; H.-J.F. and G.G. found the new mineral; H.-J.F. conducted the electron-microprobe analyses; L.B. performed the X-ray structural investigations; C.J.S. and G.G. determined the optical and physical properties; H.-J.F. wrote the paper.

Funding: This research received no external funding.

Acknowledgments: The research was supported by "progetto d'Ateneo 2015, University of Firenze" to L.B. C.J.S. acknowledges Natural Environment Research Council grant NE/M010848/1 Tellurium and Selenium Cycling and Supply. Oona Appelt (GFZ) provided assistance with the electron-microprobe work. Constructive comments of two anonymous reviewers helped to improve the paper.

Conflicts of Interest: The authors declare no conflict of interest.

References

1. Paar, W.H.; Cooper, M.A.; Moëlo, Y.; Stanley, C.J.; Putz, H.; Topa, D.; Roberts, A.C.; Stirling, J.; Raith, J.G.; Rowe, R. Eldragónite, $Cu_6BiSe_4(Se)_2$, a new mineral species from the El Dragón mine, Potosí, Bolivia, and its crystal structure. *Can. Mineral.* **2012**, *50*, 281–294. [CrossRef]
2. Mills, S.J.; Kampf, A.R.; Christy, A.G.; Housley, R.M.; Thorne, B.; Chen, Y.; Steele, I.M. Favreauite, a new selenite mineral from the El Dragón mine, Bolivia. *Eur. J. Mineral.* **2014**, *26*, 771–781. [CrossRef]
3. Förster, H.-J.; Bindi, L.; Stanley, C.J. Grundmannite, $CuBiSe_2$, the Se-analogue of emplectite: A new mineral from the El Dragón mine, Potosí, Bolivia. *Eur. J. Mineral.* **2016**, *28*, 467–477. [CrossRef]
4. Förster, H.-J.; Bindi, L.; Stanley, C.J.; Grundmann, G. Hansblockite, $(Cu,Hg)(Bi,Pb)Se_2$, the monoclinic polymorph of grundmannite, a new mineral from the Se mineralization at El Dragón (Bolivia). *Mineral. Mag.* **2017**, *81*, 629–640. [CrossRef]
5. Kampf, A.R.; Mills, S.J.; Nash, B.P.; Thorne, B.; Favreau, G. Alfredopetrovite: A new selenite mineral from the El Dragón mine. *Eur. J. Mineral.* **2016**, *28*, 479–484. [CrossRef]
6. Förster, H.-J.; Bindi, L.; Grundmann, G.; Stanley, C.J. Quijarroite, $Cu_6HgPb_2Bi_4Se_{12}$, a new selenide from the El Dragón mine, Bolivia. *Minerals* **2016**, *6*, 123. [CrossRef]
7. Bindi, L.; Förster, H.-J.; Grundmann, G.; Keutsch, F.N.; Stanley, C.J. Petříčekite, $CuSe_2$, a new member of the marcasite group from the Předbořice deposit, Central Bohemia Region, Czech Republic. *Minerals* **2016**, *6*, 33. [CrossRef]

8. Grundmann, G.; Förster, H.-J. Origin of the El Dragón selenium mineralization, Quijarro province, Potosí, Bolivia. *Minerals* **2017**, *7*, 68. [CrossRef]
9. Dymkov, Y.M.; Ryzhov, B.I.; Begizov, V.I.; Dubakina, L.S.; Zav'yalov, E.N.; Ryabeva, V.G.; Tsvetkova, M.V. Mgriite, bismuth petrovicite and associated selenides from carbonate veins of the Erzgebirge. *Novye Dannye o Mineralakh* **1991**, *37*, 81–101. (In Russian)
10. Jambor, J.L.; Pertsev, N.N.; Roberts, A.C. New mineral names. *Amer. Mineral.* **1995**, *80*, 845–850.
11. IMA-CNMNC proposal. 2018; submitted.
12. Johan, Z.; Picot, P.; Ruhlmann, F. The ore mineralogy of the Otish Mountains uranium deposit, Quebec: Skippenite, Bi_2Se_2Te, and watkinsonite, $Cu_2PbBi_4(Se,S)_8$, two new mineral species. *Can. Mineral.* **1987**, *25*, 625–638.
13. Heinrich, K.F.J.; Newbury, D.E. *Electron Probe Quantitation*; Plenum Press: New York, NY, USA, 1991.
14. Oxford Diffraction. *CrysAlis RED (Version 1.171.31.2) and ABSPACK in CrysAlis RED*; Oxford Diffraction Ltd.: Oxfordshire, UK, 2006.
15. Edenharter, A.; Nowacki, W.; Takéuchi, Y. Verfeinerung der Kristallstruktur von Bournonit $[(SbS_3)_2 \mid Cu^{IV}{}_2Pb^{VII}Pb^{VIII}]$ und von Seligmannit $[(AsS_3)_2 \mid Cu^{IV}{}_2Pb^{VII}Pb^{VIII}]$. *Z. Krist.* **1970**, *131*, 397–417. [CrossRef]
16. Maslon, E.N.; Fox, A.G.; O'Keefe, M.A. Mathematical, physical and chemical tables. In *International Tables for Crystallography*; Wilson, A.J.C., Ed.; Kluwer Academic: Dordrecht, The Netherlands, 1992; Volume C.
17. Breese, N.E.; O'Keeffe, M. Bond-Valence parameters for solids. *Acta Cryst.* **1991**, *B47*, 192–197. [CrossRef]
18. Čech, F.; Vavřín, I. Součekite, $CuPbBi(S,Se)_3$, a new mineral of the bournonite group. *Neues Jahrbuch für Mineralogie, Monatshefte* **1979**, *1979*, 289–295.
19. Simon, G.; Kesler, S.E.; Essene, E.J. Phase relations among selenides, sulphides, tellurides, and oxides: II. Applications to selenide-bearing ore deposits. *Econ. Geol.* **1997**, *92*, 468–484. [CrossRef]